HHS Public Access

Author manuscript

Chem. Author manuscript; available in PMC 2018 April 13.

Published in final edited form as:

Chem. 2017 April 13; 2(4): 550–560. doi:10.1016/j.chempr.2017.02.007.

Bright long-lived luminescence of silicon nanocrystals sensitized by two-photon absorbing antenna

Luca Ravotto[a], **Qi Chen**[b], **Yuguo Ma**[b], **Sergei A. Vinogradov**[c,*], **Mirko Locritani**[a], **Giacomo Bergamini**[a], **Fabrizia Negri**[a], **Yixuan Yu**[d], **Brian A. Korgel**[d,*], and **Paola Ceroni**[a,*]

[a]Department of Chemistry "Giacomo Ciamician", University of Bologna, Via Selmi 2, 40126 Bologna, Italy

[b]Center for Soft Matter Science and Engineering, Key Lab of Polymer Chemistry & Physics of Ministry of Education, College of Chemistry, Peking University, Beijing, 100871 (China)

[c]Departments of Biochemistry and Biophysics and Chemistry, University of Pennsylvania, Philadelphia, PA 19104, USA

[d]Department of Chemical Engineering and Texas Materials Institute, University of Texas at Austin, Austin, TX 78712, USA

Summary

Silicon nanocrystals of the average diameter of 5 nm, functionalized with 4,7-di(2-thienyl)-2,1,3-benzothiadiazole chromophores (**TBT**) and dodecyl chains, exhibit near-infrared emission upon one-photon (1P) excitation at 515 nm and two-photon (2P) excitation at 960 nm. By using **TBT** chromophores as an antenna we were able to enhance both 1P and 2P absorption cross-sections of the silicon nanocrystals to more efficiently excite their long-lived luminescence. These results chart a path to two-photon-excitable imaging probes with long-lived oxygen-independent luminescence - a rare combination of properties that should allow for a substantial increase in imaging contrast.

ETOC Blurb

Silicon nanocrystals with an average diameter of 5 nm have been functionalized with dye molecules at their surfaces. The resulting nanostructures work as molecular light-harvesting antennae: upon one-photon (1P) excitation at 515 nm or two-photon (2P) excitation at 960 nm of the peripheral dyes, the excitation energy is funneled to the silicon core and results in the sensitized emission in the near-infrared spectral region. The resulting emission is long-lived and oxygen-independent: two important properties for a substantial increase in imaging contrast.

Lead contact: paola.ceroni@unibo.it

Experimental Procedures. Full experimental procedures are provided in the Supplemental Information.

Author Contributions. P.C., S. A. V. and B. A. K. conceived the project. Q. C. and Y. M. synthesized the dye. M. L., Y. Y. and B. A. K. synthesized the Si nanocrystals. L. R., G. B. and P. C. conducted photophysical characterization and analysis. L. R., S. A. V. and P. C. performed 2P excitation experiments. F. N. performed the computational studies. All authors participated in writing the manuscript.

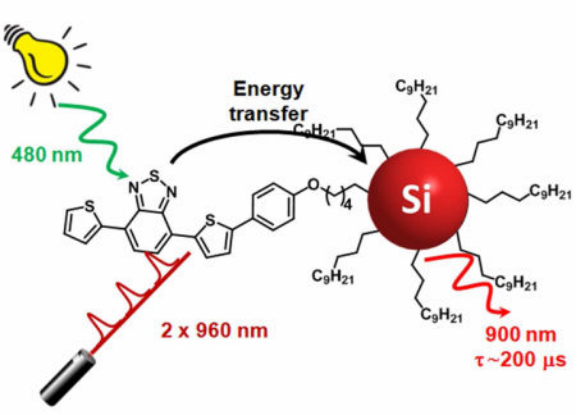

Introduction

Silicon nanocrystals (SiNCs) are an emerging class of luminescent materials,[1–5] whose optical properties can be tuned by varying the nanocrystal size.[1,2,6] The key features that inspire interest in SiNCs include the high natural abundance of silicon, lack of any known biological toxicity of Si nanoparticles [7–11] and ease of their surface passivation, which is necessary to prevent nanocrystals' oxidation and can be achieved by covalently linking protecting layers directly to silicon.[12,13] The most interesting and perhaps the most potentially useful feature of SiNCs is their bright long-lived (tens-to-hundreds of microseconds) luminescence.[14–17] Presently, there are only three other types of luminescent materials possessing this property: 1) phosphorescent complexes of some transition metals (e.g. Pt and Pd porphyrins, $[Ru(bpy)_3]^{2+}$ and alike etc); 2) molecular complexes of lanthanides; and 3) lanthanide-based upconverting nanoparticles (UCNPs). The emission of the first group of compounds is highly oxygen-sensitive, as it originates in the triplet spin states. Consequently, the emission intensities and decay times vary greatly with oxygenation, complicating quantitative imaging of probes' distributions in hetergeneously oxygenated biological environments. In addition, triplet emitters are potentially phototoxic, since their excitation leads to generation of singlet oxygen. Emission from lanthanide ions is oxygen-insensitive, but it is highly quenched by OH, NH and CH vibrations. The luminescence of UCNPs is oxygen-insensitive and is much less quenched than that of naked lanthanide ions, but the emission quantum yields of UCNPs are extremely low (in the order of 10^{-3}–10^{-4}). It follows that SiNCs occupy a unique niche,[1,5,18] possessing simultaneously microsecond lifetimes, high emission quantum yields and being insensitive to quenching neither by oxygen nor by bond vibrations. This rare combination of properties provides a strong incentive for further development of SiNCs as a platform for construction of imaging materials.

While having useful emission properties, SiNCs are rather weak light absorbers, which is explained by the indirect nature of the band gap in silicon-based materials.[19,20] Low absorption limits the luminescence brightness of Si nanocrystals, i.e. the product of the molar absorption coefficient at the excitation wavelength and the emission quantum yield. SiNCs are most efficiently excited in the UV region (300–400 nm; $\varepsilon = 5 \times 10^5\ M^{-1}\ cm^{-1}$ at 400 nm for SiNCs of 5 nm diameter),[6] while emitting in the red (λ_{max} = 650 nm). To

enhance the absorption cross-sections, SiNCs can be decorated at the surface by antenna chromophores capable of funneling excitation energy to the SiNC core. Molecular light-harvesting antennae have been widely explored in the area of colloidal semiconductor nanocrystals, e.g. CdSe.[21,22] However, up to now only a few studies have examined energy transfer as a means to induce light emission from SiNCs.[14,18,23,24]

Because UV radiation is damaging to biological tissues, development of methods for excitation of SiNCs in the near-infrared (NIR) region of the spectrum is a necessary step towards their application in bioimaging. To this end, one attractive possibility is presented by two-photon (2P) excitation[25–28] - a non-linear optical technique, whose main advantages include increased depth of imaging, higher spatial resolution and reduced tissue photodamage. Unfortunately, SiNCs exhibit quite low two-photon absorption (2PA) cross sections, as one would expect based on the indirect band gap nature of their electronic transitions. For example, the 2PA spectrum observed for SiNCs (average diameter 3 nm) in hexane (Figure S8) shows rather moderate 2PA cross-section values ($\sigma^{(2)}$), which are comparable to those of conventional fluorescent dyes,[29,30] while being 3–4 orders of magnitude lower than the cross-sections of colloidal nanocrystals.[31–35]

One approach to increase 2PA cross-sections of SiNCs is to attach multiple two-photon absorbing chromophores to their surfaces, forming a 2P light-harvesting antenna. This approach has been successfully employed, for example, in construction of 2P-ehanced dendrimeric scaffolds,[36–41] or porous silicon nanoparticles.[42,43] To the best of our knowledge, no example exists today of emission of SiNCs sensitized by 2P antennae. In the present paper, we demonstrate that covalently linking 2PA chromophores based on 4,7-di(2-thienyl)-2,1,3-benzothiadiazole (hereafter named **TBT**) to SiNCs is a viable route to enhance their luminescence upon NIR excitation. As a result, multiphoton excitation becomes combined in SiNCs with their microsecond-scale luminescence, paving a path to imaging probes with unprecendently high imaging contrast.

Results and discussion

Synthesis and structural characterization

TBT was synthesized and characterized as described in the Supporting Information (Figure S1 and S2).

SiNCs can be conveniently synthesized by thermal decomposition of hydrogen silsesquioxane (HSQ) at 1200°C to give oxide-embedded silicon nanocrystals that are liberated by etching and then passivated by thermal hydrosilylation using terminal alkenes (Scheme 1).[44,45] Thus produced SiNCs have controllable size, high monodispersity, passivated surface, good dispersibility in organic solvents and high stability.[14,45,46] In the present study, the SiNCs were passivated with a mixture of 1-dodecene and **TBT** (dodecene:**TBT** molar ratio of 52:1), giving modified nanocrystals (hereafter named **Si-TBT**). The length of the bridge which links the chromophore to the silicon nanocrystal is a key parameter for the energy transfer efficiency, as we have previously investigated in the case of pyrene chromophores.[23] The current length represents a good compromise to obtain a high efficiency of energy transfer (see below) and a good degree of

functionalization of SiNC surface. Indeed, chromophore molecules are bulkier than alkyl chains, and when connecting linkers are short, coverage of the SiNC surfaces may be poor due to the steric constraints, and the luminescence quantum yield may be strongly diminished as a consequence.

For control and comparison, SiNCs were also passivated using 1-dodecene only (hereafter named **Si**). The resulting materials were purified by centrifugation (8000 rpm for 5 min, corresponding to a relative centrifugal force of 8230 G), after which the precipitate, containing poorly capped and thus less soluble SiNCs was removed. The supernatant was purified by several centrifugation/precipitation cycles using toluene/ethanol solvent-antisolvent pair. The final samples were dispersed in toluene. A sample of SiNCs capped by dodecyl chains and dispersed in hexane was used for measurements of 2P absorption spectrum and it was available from previous studies.[23] Characterization of the silicon nanocrystals was performed by transmission electron microscopy and FTIR spectroscopy (see Figure S3 and S4).

Photophysical properties of TBT

Compound **TBT** is a π-conjugated donor-acceptor-donor chromophore comprising two thiophene donor units and a benzothiadiazole acceptor unit. The symmetry of **TBT** is broken, since one of the thiophenes carries an additional electron-donating methoxyphenyl substituent. **TBT** has high molar absorption coefficient in the blue region of the spectrum (Figure 1a, black line) and strong fluorescence, e.g. in toluene with maximum at 620 nm and the quantum yield of 83%. Upon increase in the solvent polarity, **TBT** exhibits a small shift of the absorption band (Figure S7) and a large red-shift of the emission (Figure 1b), e.g. from 580 to 674 nm in going from hexane to dimethylsulfoxide. This red shift of the fluorescence is accompanied by a decrease in the quantum yield: from 92% to 42% in going from hexane to dimethylsulfoxide. Such strong solvatofluorism as well as the large Stokes shift between the absorption and emission maxima are an indication of a strongly polar excited state.

2PA spectra were measured by the two-photon excitation method, whereby the sample was excited by a continuous train of femtosecond pulses from a tunable Ti:sapphire laser oscillator (80 MHz rep. rate), and the emission was registered by a CCD-based spectrometer (see SI and ref. [47] for details). After normalization and correction (see SI for details), the plot of the integrated emission intensity *vs* excitation wavelength gave the relative 2PA absorption spectrum. The latter was referenced to the 2PA spectrum of a standard (Rhodamine B in MeOH), for which 2PA cross-sections was known from the literature. [48,49] At each excitation wavelength, the dependence of the emission signal on the excitation flux was confirmed to be quadratic (see Figure S9).

The 2PA spectrum of **TBT** is shown in Figure 1a, red line. The lowest energy transition ($S_0 \rightarrow S_1$, 480 nm) shows a small 2PA cross-section ($\sigma^{(2)}$<10 GM), while there is a much stronger 2P band ($\sigma^{(2)}$ = 150 GM) at 365 nm (λ^{2P}=730 nm).

Modeling structural and optical properties of TBT

To assist the analysis of the 1P and 2P spectra of **TBT**, quantum chemical calculations were carried out on a symmetric model, which lacks the alkoxybenzene moiety (hereafter named **mTBT**), and on the target molecule (see Scheme 2).

To inspect the nature of the excited states and to evaluate the excitation energies, TD-CAM-B3LYP/6-31G** calculations were carried out for **mTBT** and **TBT**. According to the calculations, the lowest energy absorption band in the spectra of both chromophores is dominated by the HOMO-LUMO (H→L) single-electron excitation. As shown in Figure S5, the HOMO is substantially delocalized over the entire chromophore, while the LUMO is localized primarily on the acceptor moiety, thereby conveying a partial charge transfer character to the lowest excited state (S_1). For **TBT** the static dipole moment of S_1 is calculated to be 7.25 D at the ground state geometry, compared to 1.97 D in the ground state. The equilibrium structure of the lowest excited state of **TBT** was also computed (see Figure S6), and the dipole moment in this geometry retains the large value of 6.69 D. Therefore, the strong sensitivity to solvent polarity of the **TBT** emission energy can be associated with the higher polarity of the lowest excited state compared to the ground state.[50]

For both **mTBT** and **TBT**, the second singlet excited state (S_2) was found to be dominated by (H-1→L) excitation. For **TBT** this excited state also exhibits charge transfer character and a large static dipole moment of 6.77 D (computed for ground state geometry). The computed oscillator strength $f(S_0 \rightarrow S_2)$ is negligible for **mTBT** (Table S1) and quite small also for **TBT** (Table 1). The second experimentally observed intense transition in the linear (one-photon) absorption spectrum of **TBT** is therefore attributed to a higher excited singlet state (S_3) and similarly in **mTBT**. The $S_1 \rightarrow S_3$ transition is dominated by the (H→L+1) excitation, having a weaker charge transfer character. The static dipole moment of **TBT** in S_3 is computed to be 4.60 D at the ground state geometry. A comparison of the experimental and computed one-photon absorption spectra of **TBT** is shown in Figure 2.

Thus, the second absorption band in the 1P spectrum of **TBT** encompasses two electronic transitions. In light of this observation we note that the maximum of the 2P transition (Figure 1) overlaps with the shoulder of the broad 1P band (λ_{max}=335 nm), suggesting that the second of the three lowest excited states of **TBT** (and **mTBT**) can be more 2P-active.

Considering a chromophore with a centrosymmetrical structure, its 2PA properties may be described by the well-known three-state model,[51] whereby the S_1 state plays the role of the key intermediate state promoting 2P transition to a higher two-photon active state (presumably $S_0 \rightarrow S_2$).[52] The large value of the transition dipole moment for $S_0 \rightarrow S_1$ excitation and the proximity of the laser energy to the S_1 energy when the laser is at resonance with the 2P state (presumably S_2) would both contribute to the enhancement of 2PA in symmetrical dyes, such as **mTBT**.[53,54] In addition, large difference between the static dipole moments in the ground and final 2P states may also be a factor increasing the strength of the corresponding transition as shown by the following simplified equation for 2PA:[55]

$$M_{1\to f}^{(2)} \propto \frac{(\mu_{ff}-\mu_{ii})\,\mu_{if}}{\mathrm{h}\omega} - \sum_{p\neq i,f}\frac{\mu_{fp}\mu_{pi}}{\mathrm{h}\omega - E_{pi}} \quad (1)$$

where $\hbar\omega$ is the photon energy, μ_{ff} and μ_{ii} are permanent moments of the final and initial states and μ_{pi} and μ_{fp} are transition dipole moments involving the intermediate state *p* whose excitation energy is E_{pi}.

The computed 2PA cross-sections for the four lowest excited states are collected in Table 1 for **TBT** and Table S1 for **mTBT**. The lowest excited states of both **TBT** and **mTBT** display modest 2P activity, which agrees with our experiments. The transition to the second excited state (S_2), which is characterized by a low oscillator strength, shows quite large 2PA activity, that is further enhanced in going from symmetrical **mTBT** to less symmetrical **TBT** system. The four lowest energy transitions of **mTBT** exhibit alternating 1PA/2PA pattern,[53] indicating that the selection rules for centrosymmetrical molecules still prevails in spite of the lack of an inversion center, as observed for other non-centrosymmetrical chromophores.[56] The enhancement of the 2PA of S_2 in **TBT** vs **mTBT** may be attributed to the contribution of the static dipole moment terms in eq. (1) considering that the transition dipole moment to S_2 is negligible for **mTBT** and not for **TBT**.

Photophysical properties of Si-TBT

Given that a large number of **TBT** moieties are attached to each nanocrystal in **Si-TBT** conjugates, we set out to investigate whether **TBT** arrays can act as an antenna, capable of sensitizing emission of SiNCs. The linear absorption spectrum of **Si-TBT** in toluene (black line in Figure 3a) is nearly a superposition of the **TBT** features (Figure 1a) and the typical featureless absorption of SiNCs (red line in Figure 3a), suggesting that these two electronic systems are not strongly coupled neither in the ground nor in the excited states. Based on the molar absorption coefficients of the two components, on average eighteen **TBT** chromophores were estimated to be associated with each nanocrystal.[6]

Upon excitation of the **TBT** chromophore at 515 nm, strong quenching (ca. 95%) of the **TBT** fluorescence at 640 nm was observed in the **Si-TBT** system (black line in Figure 3b), as compared to the **TBT** in an optically matched mixture containing **TBT** and **Si** (green line in Figure 3b). Furthermore, the lifetime of the fluorescent excited state of **TBT** was found to be strongly decreased (ca. 95%), i.e. from 7.9 ns for the free chromophore in toluene to 0.4 ns when **TBT** was bound to SiNCs.[⊥] Concomitantly, sensitized NIR long-lived emission of SiNCs was observed (Figure 3b, τ=160 μs at 800 nm), confirming that the light absorbed by **TBT** sensitizes emission of the SiNC core. The sensitization was further confirmed by running time-delayed excitation spectra (λ_{em}=800 nm) with emission collected 40 μs after the excitation pulse, when all the prompt signals have already decayed (inset of Figure 3a), and only the long-lived emission signals last. The efficiency of the sensitization was estimated to be ca. 75% (see Supporting Information and Figure S11 for details).

[⊥]The fluorescence decay of **Si-TBT** was fitted by a biexponential curve since a small fraction of free **TBT** was present in the sample (ca. 10%).

Excitation of **Si-TBT** at 390 nm, where most (>95%) of the light is absorbed by the silicon core, resulted in the near-infrared emission with the quantum yield of 23%, as compared to 45% for dodecyl-capped **Si**.[≠] A decrease in the quantum yield has been reported previously for silicon nanocrystals modified with other organic dyes,[14,24] and it can be related to an increase in the number of defects at the nanocrystals' surfaces due to the steric bulk of the chromophore moieties that preclude homogeneous passivation by an alkyl layer.

Upon excitation at 515 nm, the brightness of **Si-TBT** is 2 times higher compared to **Si**.

It is worth a note that **TBT** chromophore is not only an efficient sensitizer of the SiNC emission, but also its fluorescence maximum is indicative of the polarity of the environment, e.g. shifting from 590 to 640 nm in going from hexane to dichloromethane.

Sensitization of the SiNC emission upon excitation of **Si-TBT** near the maximum of the 2PA spectrum (730 nm) turned out to be impossible to quantify because of the strongly interfering one-photon absorption by the silicon core itself. Although the linear absorption cross-section of SiNC at 730 nm is very small, extremely high excitation flux produced by the ultrafast laser pulses made the contribution of this linear absorption dominant and the power dependence of the emission strictly linear. In contrast, excitation of **Si-TBT** at 960 nm (Figure S12), despite the low 2PA cross-section at that wavelength, resulted in a clearly observable luminescence, characterized by a close to quadratic power dependence (see inset in Figure 4). The decay of the luminescence intensity of the SiNC core (emission integrated for λ_{em}<900 nm) upon excitation of **Si-TBT** at 960 nm is shown in Figure 4 (black line) along with the decay of the luminescence of **Si** alone (red line). Although the latter emission is observable, the luminescence of **Si-TBT** is much stronger due to the enhancement effect of the **TBT** antenna. The average decay times of the luminescence of **Si** and **Si-TBT** were found to be different, whereby the luminescence of **Si-TBT** was decaying faster, reflecting its lower quantum yield.

In order to quantify the antenna effect, the decays were measured using sample solutions containing equal concentrations of SiNCs, i.e. solutions isoabsorbing at 390 nm (Figure 3a). Upon excitation by pulses of equal power, the initial intensities of the luminescence signals of **Si** and **Si-TBT** in such samples should be proportional to the initially created excited state populations and therefore to the absorption rate constants. The initial intensity of the luminescence of **Si-TBT** was found to be two times higher than that of **Si**, demonstrating two-fold increase in the 2PA. The increase in the power dependence slope in going from **Si** to **Si-TBT** (Figure 4) indicates higher contribution of 2PA in the case of **Si-TBT** as result of this antenna effect.

Because of the instrument limitations, it was not possible to measure the 2PA spectrum of the **Si** and **Si-TBT** samples in order to make a comparison of 2P cross sections in a wide spectral range. However, the low 2P cross-section of SiNCs[25] is confirmed by the 2PA

[≠]In order to compare the photophysical properties as a function of the dimension of the silicon core, the same experiments were performed also for SiNC with average diameter of 3 nm (see SI and Figure S10 for details).

spectrum measured from a sample of dodecyl capped SiNCs with 3 nm diameter dispersed in hexane (Figure S8).

Conclusions

Silicon nanocrsytals have recently emerged as a new class of luminescent materials for light-emitting diodes, sensing and bioimaging. In order to make them suitable for biomedical applications a number of requirements have to be met, starting with increasing their efficiency in absorbing light at the visible-NIR range limit as well as proving their stability in water. Here, we demonstrated that surface functionalization of luminescent SiNCs with multiple (18 per nanoparticle, as an average) dithienyl-benzothiadiazole chromophores (**TBT**) effectively increases the SiNCs apparent 1P and 2P absorption cross-sections. Upon excitation of the **TBT** antenna in the visible spectral region (λ_{max} = 480 nm) efficient energy transfer (η=75%) sensitizes NIR emission of SiNC (λ_{max}= 920 nm). Moreover, because **TBT** has relatively high two-photon absorption cross section in the red and NIR spectral region, emission of the SiNC core can be sensitized also upon 2P excitation at 960 nm. In contrast, direct 2P excitation of SiNC is inefficient.

To the best of our knowledge, the present system is the first example of a light-harvesting two-photon antenna used to sensitize emission of SiNCs. This result opens up the potential for bioimaging applications, such as increased depth of imaging, higher resolution and reduced risk of photodamage, can be coupled with the bright, long-lived and oxygen-insensitive NIR luminescence of SiNCs. It is thus a rare combination of properties that allow for microsecond-scale time-gate detection: background autofluorescence and scattered excitation light can be removed by low-cost equipment, resulting in an increase of contrast and signal-to-noise ratio in images. Further studies will be devoted to optimization of the antenna system for better emission sensitization as well as to obtaining solubility of SiNCs in aqueous environments.

Supplementary Material

Refer to Web version on PubMed Central for supplementary material.

Acknowledgments

LR, ML, GB and PC gratefully acknowledge financial support by the European Commission ERC Starting Grant (PhotoSi, 278912). SAV acknowledges financial support of the grants EB018464 and NS092986 from the National Institutes of Health, USA. YY and BAK acknowledge financial support from the Robert A. Welch Foundation (F-1464) and the US National Science Foundation (CHE-1308813).

References

1. McVey BFP, Tilley RD. Solution Synthesis, Optical Properties, and Bioimaging Applications of Silicon Nanocrystals. Acc Chem Res. 2014; 47:3045–3051. DOI: 10.1021/ar500215v [PubMed: 25252604]
2. Mastronardi ML, Henderson EJ, Puzzo DP, Ozin GA. Small Silicon, Big Opportunities: The Development and Future of Colloidally-Stable Monodisperse Silicon Nanocrystals. Adv Mater. 2012; 24:5890–8. DOI: 10.1002/adma.201202846 [PubMed: 23289121]

3. Gonzalez CM, Iqbal M, Dasog M, Piercey DG, Lockwood R, Klapotke TM, et al. Detection of high-energy compounds using photoluminescent silicon nanocrystal paper based sensors. Nanoscale. 2014; 6:2608–12. DOI: 10.1039/C3NR06271F [PubMed: 24481004]
4. Yi Y, Zhu G, Liu C, Huang Y, Zhang Y, Li H, et al. A Label-Free Silicon Quantum Dots-Based Photoluminescence Sensor for Ultrasensitive Detection of Pesticides. Anal Chem. 2013; 85:11464–70. DOI: 10.1021/ac403257p [PubMed: 24160846]
5. Dasog M, Kehrle J, Rieger B, Veinot JGC. Silicon nanocrystals and silicon-polymer hybrids: Synthesis, surface engineering, and applications. Angew Chemie - Int Ed. 2016; 55:2322–39. DOI: 10.1002/anie.201506065
6. Hessel CM, Reid D, Panthani MG, Rasch MR, Goodfellow BW, Wei J, et al. Synthesis of Ligand-Stabilized Silicon Nanocrystals with Size-Dependent Photoluminescence Spanning Visible to Near-Infrared Wavelengths. Chem Mater. 2012; 24:393–401. DOI: 10.1021/cm2032866
7. Alsharif NH, Berger CEM, Varanasi SS, Chao Y, Horrocks BR, Datta HK. Alkyl-capped silicon nanocrystals lack cytotoxicity and have enhanced intracellular accumulation in malignant cells via cholesterol-dependent endocytosis. Small. 2009; 5:221–8. DOI: 10.1002/smll.200800903 [PubMed: 19058285]
8. Ruizendaal L, Bhattacharjee S, Pournazari K, Rosso-Vasic M, de Haan LHJ, Alink GM, et al. Synthesis and cytotoxicity of silicon nanoparticles with covalently attached organic monolayers. Nanotoxicology. 2009; 3:339–47. DOI: 10.3109/17435390903288896
9. Park J-H, Gu L, von Maltzahn G, Ruoslahti E, Bhatia SN, Sailor MJ. Biodegradable luminescent porous silicon nanoparticles for in vivo applications. Nat Mater. 2009; 8:331–6. DOI: 10.1038/nmat2398 [PubMed: 19234444]
10. Bhattacharjee S, Rietjens IMCM, Singh MP, Atkins TM, Purkait TK, Xu Z, et al. Cytotoxicity of surface-functionalized silicon and germanium nanoparticles: the dominant role of surface charges. Nanoscale. 2013; 5:4870.doi: 10.1039/c3nr34266b [PubMed: 23619571]
11. McVey BFP, Prabakar S, Gooding JJ, Tilley RD. Solution Synthesis, Surface Passivation, Optical Properties, Biomedical Applications, and Cytotoxicity of Silicon and Germanium Nanocrystals. Chempluschem. 2016; doi: 10.1002/cplu.201600207
12. Buriak JM. Illuminating Silicon Surface Hydrosilylation: An Unexpected Plurality of Mechanisms. Chem Mater. 2014; 26:763–72. DOI: 10.1021/cm402120f
13. Kelly JA, Henderson EJ, Veinot JGC. Sol-gel precursors for group 14 nanocrystals. Chem Commun. 2010; 46:8704–18. DOI: 10.1039/C0CC02609C
14. Locritani M, Yu Y, Bergamini G, Baroncini M, Molloy JK, Korgel BA, et al. Silicon Nanocrystals Functionalized with Pyrene Units: Efficient Light-Harvesting Antennae with Bright Near-Infrared Emission. J Phys Chem Lett. 2014; 5:3325–9. DOI: 10.1021/jz501609e [PubMed: 26278439]
15. Rowland CE, Hannah DC, Demortière A, Yang J, Cook RE, Prakapenka VB, et al. Silicon Nanocrystals at Elevated Temperatures: Retention of Photoluminescence and Diamond Silicon to β-Silicon Carbide Phase Transition. ACS Nano. 2014; 8:9219–23. DOI: 10.1021/nn5029967 [PubMed: 25181589]
16. Zhou Z, Brus L, Friesner R. Electronic Structure and Luminescence of 1.1- and 1.4-nm Silicon Nanocrystals: Oxide Shell versus Hydrogen Passivation. Nano Lett. 2003; 3:163–7. DOI: 10.1021/nl025890q
17. Beard MC, Knutsen KP, Yu P, Luther JM, Song Q, Metzger WK, et al. Multiple Exciton Generation in Colloidal Silicon Nanocrystals. Nano Lett. 2007; 7:2506–12. DOI: 10.1021/nl071486l [PubMed: 17645368]
18. Romano F, Yu Y, Korgel BA, Bergamini G, Ceroni P. Light-Harvesting Antennae Based on Silicon Nanocrystals. Top Curr Chem. 2016; 374:1–18. DOI: 10.1007/s41061-016-0056-9
19. Hodes G. When Small Is Different: Some Recent Advances in Concepts and Applications of Nanoscale Phenomena. Adv Mater. 2007; 19:639–55. DOI: 10.1002/adma.200601173
20. Kovalev D, Diener J, Heckler H, Polisski G, Künzner N, Koch F. Optical absorption cross sections of Si nanocrystals. Phys Rev B. 2000; 61:4485–7.
21. Algar WR, Kim H, Medintz IL, Hildebrandt N. Emerging non-traditional Förster resonance energy transfer configurations with semiconductor quantum dots: Investigations and applications. Coord Chem Rev. 2014; 263–264:65–85. doi:http://dx.doi.org/10.1016/j.ccr.2013.07.015.

22. Medintz IL, Mattoussi H. Quantum dot-based resonance energy transfer and its growing application in biology. Phys Chem Chem Phys. 2009; 11:17–45. DOI: 10.1039/B813919A [PubMed: 19081907]
23. Mazzaro R, Locritani M, Molloy JK, Montalti M, Yu Y, Korgel BA, et al. Photoinduced Processes between Pyrene-Functionalized Silicon Nanocrystals and Carbon Allotropes. Chem Mater. 2015; 27:4390–7. DOI: 10.1021/acs.chemmater.5b01769
24. Fermi A, Locritani M, Di Carlo G, Pizzotti M, Caramori S, Yu Y, et al. Light-harvesting antennae based on photoactive silicon nanocrystals functionalized with porphyrin chromophores. Faraday Discuss. 2015; 185:481–95. DOI: 10.1039/C5FD00098J [PubMed: 26399301]
25. He GS, Zheng Q, Yong K-T, Erogbogbo F, Swihart MT, Prasad PN. Two- and Three-Photon Absorption and Frequency Upconverted Emission of Silicon Quantum Dots. Nano Lett. 2008; 8:2688–92. DOI: 10.1021/nl800982z [PubMed: 18698830]
26. Tu C, Ma X, Pantazis P, Kauzlarich SM, Louie AY. Paramagnetic, Silicon Quantum Dots for Magnetic Resonance and Two-Photon Imaging of Macrophages. J Am Chem Soc. 2010; 132:2016–23. DOI: 10.1021/ja909303g [PubMed: 20092250]
27. Henderson EJ, Shuhendler AJ, Prasad P, Baumann V, Maier-Flaig F, Faulkner DO, et al. Colloidally stable silicon nanocrystals with near-infrared photoluminescence for biological fluorescence imaging. Small. 2011; 7:2507–16. DOI: 10.1002/smll.201100845 [PubMed: 21739601]
28. Chandra S, Ghosh B, Beaune G, Nagarajan U, Yasui T, Nakamura J, et al. Functional double-shelled silicon nanocrystals for two-photon fluorescence cell imaging: spectral evolution and tuning. Nanoscale. 2016; 8:9009–19. DOI: 10.1039/C6NR01437B [PubMed: 27076260]
29. Pawlicki M, Collins HA, Denning RG, Anderson HL. Two-Photon Absorption and the Design of Two-Photon Dyes. Angew Chem Int Ed. 2009; 48:3244–66. DOI: 10.1002/anie.200805257
30. Terenziani F, Katan C, Badaeva E, Tretiak S, Blanchard-Desce M. Enhanced Two-Photon Absorption of Organic Chromophores: Theoretical and Experimental Assessments. Adv Mater. 2008; 20:4641–78. DOI: 10.1002/adma.200800402
31. Larson DR, Zipfel WR, Williams RM, Clark SW, Bruchez MP, Wise FW, et al. Water-soluble quantum dots for multiphoton fluorescence imaging in vivo. Science. 2003; 300:1434–6. DOI: 10.1126/science.1083780 [PubMed: 12775841]
32. Lemon CM, Karnas E, Han X, Bruns OT, Kempa TJ, Fukumura D, et al. Micelle-Encapsulated Quantum Dot-Porphyrin Assemblies as in Vivo Two-Photon Oxygen Sensors. J Am Chem Soc. 2015; 137:9832–42. DOI: 10.1021/jacs.5b04765 [PubMed: 26149349]
33. Qi Z-D, Li D-W, Jiang P, Jiang F-L, Li Y-S, Liu Y, et al. Biocompatible CdSe quantum dot-based photosensitizer under two-photon excitation for photodynamic therapy. J Mater Chem. 2011; 21:2455.doi: 10.1039/c0jm03229h
34. Martinez Maestro L, Martin Rodriguez E, Sanz Rodriguez F, Iglesias-de la Cruz MC, Juarranz A, Naccache R, et al. CdSe Quantum Dots for Two-Photon Fluorescence Thermal Imaging. Nano Lett. 2010; 10:5109–15. DOI: 10.1021/nl1036098 [PubMed: 21062040]
35. Jin H, Gui R, Sun J, Wang Y. Ratiometric two-photon excited photoluminescence of quantum dots triggered by near-infrared-light for real-time detection of nitric oxide release in situ. Anal Chim Acta. 2016; 922:48–54. DOI: 10.1016/j.aca.2016.03.052 [PubMed: 27154831]
36. He GS, Lin T-C, Cui Y, Prasad PN, Brousmiche DW, Serin JM, et al. Two-photon excited intramolecular energy transfer and light-harvesting effect in novel dendritic systems. Opt Lett. 2003; 28:768–70. DOI: 10.1364/OL.28.000768 [PubMed: 12779140]
37. Briñas RP, Troxler T, Hochstrasser RM, Vinogradov SA. Phosphorescent Oxygen Sensor with Dendritic Protection and Two-Photon Absorbing Antenna. J Am Chem Soc. 2005; 127:11851–62. DOI: 10.1021/ja052947c [PubMed: 16104764]
38. Wan Y, Yan L, Zhao Z, Ma X, Guo Q, Jia M, et al. Gigantic two-photon absorption cross sections and strong two-photon excited fluorescence in pyrene core dendrimers with fluorene/carbazole as dendrons and acetylene as linkages. J Phys Chem B. 2010; 114:11737–45. DOI: 10.1021/jp104868j [PubMed: 20735053]

39. Mongin O, Krishna TR, Werts MH, Caminade AM, Majoral JP, Blanchard-Desce M. A modular approach to two-photon absorbing organic nanodots: brilliant dendrimers as an alternative to semiconductor quantum dots? Chem Commun. 2006; :915–7. DOI: 10.1039/b517270e
40. Roussakis E, Spencer JA, Lin CP, Vinogradov SA. Two-photon antenna-core oxygen probe with enhanced performance. Anal Chem. 2014; 86:5937–45. DOI: 10.1021/ac501028m [PubMed: 24848643]
41. Lin TC, Lin WL, Wang CM, Fu CW. Synthesis and characterization of highly soluble two-photon-absorbing chromophores with multi-branched and dendritic architectures. European J Org Chem. 2011; :912–21. DOI: 10.1002/ejoc.201001165
42. Secret E, Maynadier M, Gallud A, Chaix A, Bouffard E, Gary-Bobo M, et al. Two-Photon Excitation of Porphyrin-Functionalized Porous Silicon Nanoparticles for Photodynamic Therapy. Adv Mater. 2014; 26:7643–8. DOI: 10.1002/adma.201403415 [PubMed: 25323443]
43. Knežević NŽ, Stojanovic V, Chaix A, Bouffard E, Cheikh K El, Morère A, et al. Ruthenium(ii) complex-photosensitized multifunctionalized porous silicon nanoparticles for two-photon near-infrared light responsive imaging and photodynamic cancer therapy. J Mater Chem B. 2016; 4:1337–42. DOI: 10.1039/C5TB02726H
44. Hessel CM, Henderson EJ, Veinot JGC. Hydrogen Silsesquioxane: A Molecular Precursor for Nanocrystalline Si−SiO2 Composites and Freestanding Hydride-Surface-Terminated Silicon Nanoparticles. Chem Mater. 2006; 18:6139–46. DOI: 10.1021/cm0602803
45. Hessel CM, Rasch MR, Hueso JL, Goodfellow BW, Akhavan VA, Puvanakrishnan P, et al. Alkyl Passivation and Amphiphilic Polymer Coating of Silicon Nanocrystals for Diagnostic Imaging. Small. 2010; 6:2026–34. DOI: 10.1002/smll.201000825 [PubMed: 20818646]
46. Panthani MG, Hessel CM, Reid D, Casillas G, José-Yacamán M, Korgel BA. Graphene-Supported High-Resolution TEM and STEM Imaging of Silicon Nanocrystals and their Capping Ligands. J Phys Chem C. 2012; 116:22463–8. DOI: 10.1021/jp308545q
47. Esipova TV, Rivera-Jacquez HJ, Weber B, Masunov AE, Vinogradov SA. Two-Photon Absorbing Phosphorescent Metalloporphyrins: Effects of π-Extension and Peripheral Substitution. J Am Chem Soc. 2016; 138:15648–62. DOI: 10.1021/jacs.6b09157 [PubMed: 27934026]
48. Makarov NS, Drobizhev M, Rebane A. Two-photon absorption standards in the 550–1600 nm excitation wavelength range. Opt Express. 2008; 16:4029–47. DOI: 10.1364/OE.16.004029 [PubMed: 18542501]
49. Xu C, Webb WW. Measurement of two-photon excitation cross sections of molecular fluorophores with data from 690 to 1050 nm. J Opt Soc Am B. 1996; 13:481–91. DOI: 10.1364/JOSAB.13.000481
50. Reichardt C. Solvatochromic dyes as solvent polarity indicators. Chem Rev. 1994; 94:2319–58. DOI: 10.1021/cr00032a005
51. Butcher, PN., Cotter, D. The Elements of Nonlinear Optics. Cambridge: Cambridge University Press; 1990.
52. Albota M, Beljonne D, Brédas J-L, Ehrlich JE, Fu J-Y, Heikal AA, et al. Design of Organic Molecules with Large Two-Photon Absorption Cross Sections. Science. 1998; (80-):281. [PubMed: 9765151]
53. Ellinger S, Graham KR, Shi P, Farley RT, Steckler TT, Brookins RN, et al. Donor–Acceptor–Donor-based π-Conjugated Oligomers for Nonlinear Optics and Near-IR Emission. Chem Mater. 2011; 23:3805–17. DOI: 10.1021/cm201424a
54. Kato S, Matsumoto T, Shigeiwa M, Gorohmaru H, Maeda S, Ishi-i T, et al. Novel 2,1,3-Benzothiadiazole-Based Red-Fluorescent Dyes with Enhanced Two-Photon Absorption Cross-Sections. Chem Eur J. 2006; 12:2303–17. DOI: 10.1002/chem.200500921 [PubMed: 16363008]
55. Meath WJ, Power EA. On the importance of permanent moments in multiphoton absorption using perturbation theory. J Phys B. 1984; 17:763–81. DOI: 10.1088/0022-3700/17/5/017
56. Makarov NS, Drobizhev M, Wicks G, Makarova EA, Lukyanets EA, Rebane A. Alternative selection rules for one- and two-photon transitions in tribenzotetraazachlorin: quasi-centrosymmetrical π-conjugation pathway of formally non-centrosymmetrical molecule. J Chem Phys. 2013; 138:214314.doi: 10.1063/1.4807594 [PubMed: 23758378]

The bigger picture

Silicon nanocrystals (SiNCs) occupy a niche in the realm of quantum dots, offering several advantages: silicon is abundant, essentially non-toxic and can form robust chemical bonds with ligands at the nanocrystal surface. From the optical point of view, SiNCs are strong light emitters, but weak absorbers. The latter drawback was circumvented by their surface functionalization with chromophores that are strong light absorbers and are able to efficiently transfer the excitation energy to the silicon core. Here, we present a step further: functionalization of SiNCs with multiple two-photon absorbing chromophores, forming a 2P light-harvesting antenna. The 2P antenna enables excitation of SiNCs in the near-infrared (NIR) region of the spectrum, charting a path to applications in bioimaging. Long-lived oxygen-insensitive luminescence and two-photon excitability is a rare combination of properties, which may allow unprecedentedly high contrast in images from scattering biological tissues.

Highligths

Silicon nanocrystals (SiNCs) are weak light absorbers, but highly luminescent

Excitation of benzothiadiazole chromophores attached to SiNCs sensitizes core emission

An antenna by 2-photon excitation is coupled to long-lived SiNC luminescence

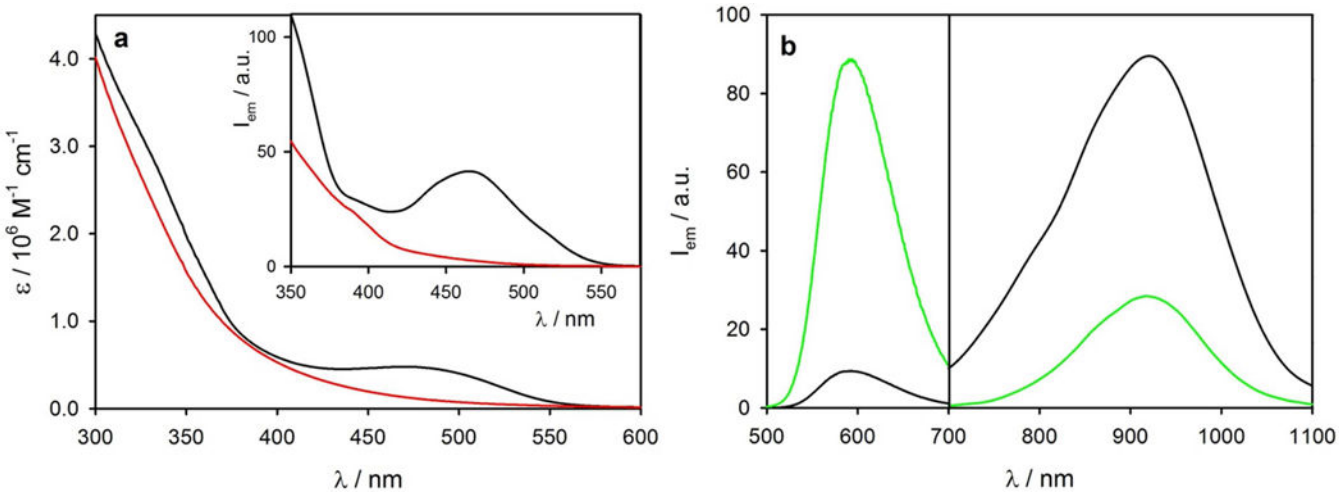

Figure 1. Photophysical properties of TBT

(a) 1P (black line, referred to black axes) and 2P absorption (red line, referred to red axes) of **TBT** in toluene at room temperature. (b) Normalized emission spectra of **TBT** in solvents of different polarity. λ_{ex} = 470 nm.

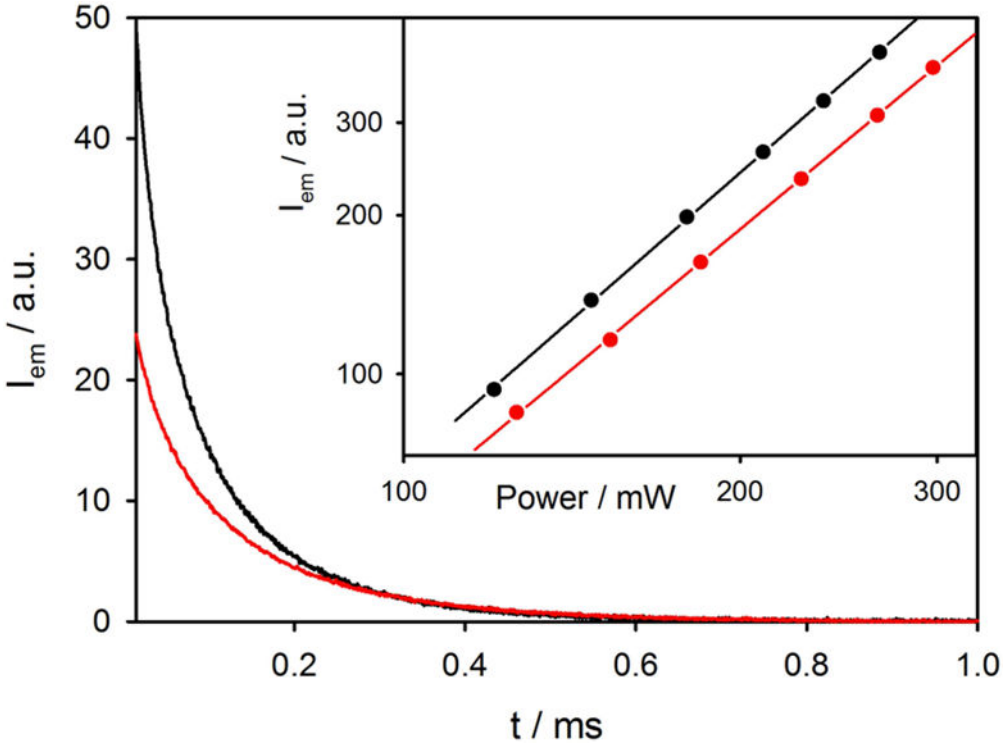

Figure 2. Computed and experimental absorption spectrum of TBT

TDDFT/CAM-B3LYP/6-31G** computed (bottom) and experimental (top) one photon absorption spectrum of **TBT**. The simulated spectrum shows the lowest three electronic transitions, broadened by Lorenzian functions chosen to facilitate visual comparison with the experimental spectrum. The orbitals participating in the leading excitations are also shown.

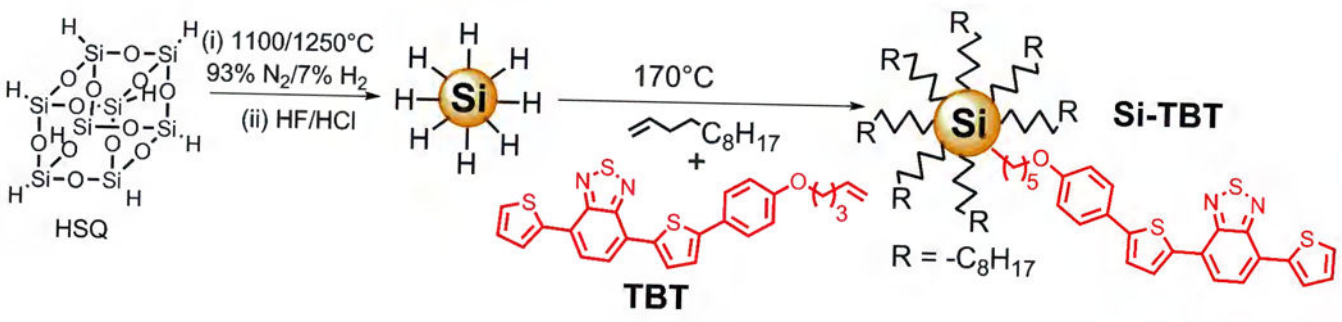

Figure 3. Photophysical properties of Si-TBT

(a) Absorption spectra of **Si-TBT** (black line) and **Si** (red line) in toluene. (b) Emission spectrum of **Si-TBT** (black line) (λ_{ex}=515 nm) compared to that of an optically matched solution (at 515 nm) of **Si** and **TBT** (green line) in toluene. Inset shows time-delayed (Δt=40 μs) excitation spectra of **Si-TBT** and **Si** in toluene (λ_{em} = 800 nm).

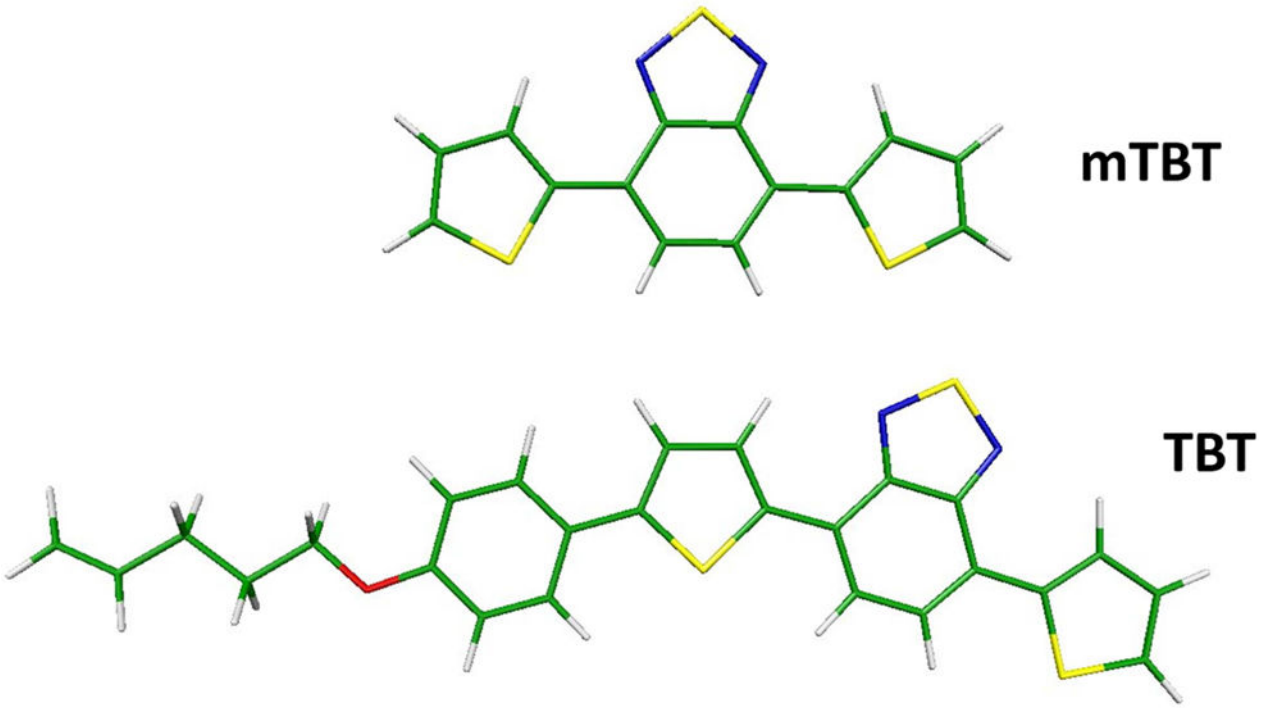

Figure 4. 2P excitation of Si-TBT vs Si

Decay of emission intensity of **Si-TBT** (black line) and **Si** (red line) at λ_{em}<900 nm upon two-photon excitation at 960 nm. Inset shows the dependence of the 2PA signal on the laser power: slopes are 1.85 and 1.74 for **Si-TBT** and **Si**, respectively.

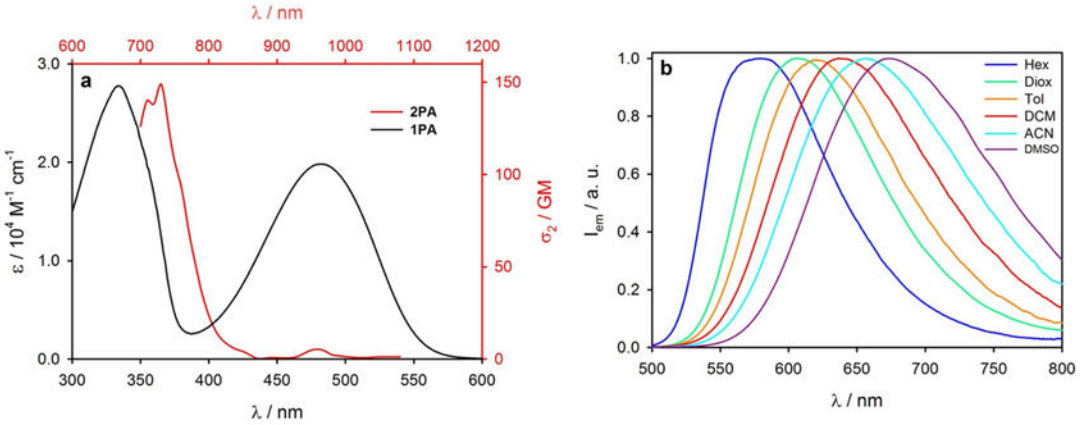

Scheme 1.

Synthesis and functionalization of **Si-TBT**.

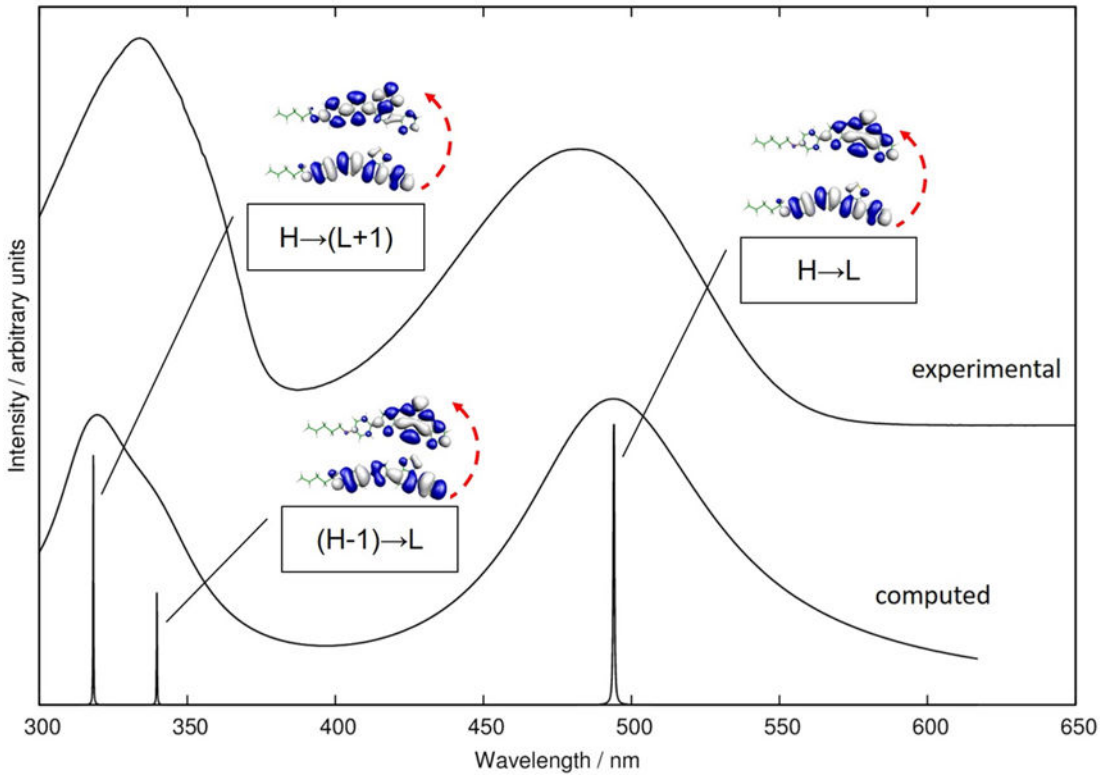

Scheme 2.

Structures of the lowest energy conformers of **mTBT** and **TBT**.

Table 1

One photon and two photon absorption properties of **TBT** from TD-CAM-B3LYP/6-31G** calculations.

Excited state	λ_{abs}/nm[a]	$\sigma^{(2)}$/GM[b]	f[c]	Wavefunction composition
S_1	494	54	0.74	(H→L)
S_2	340	1010	0.26	(H-1→L)
S_3	318	1710	0.56	(H→L+1)
S_4	292	620	0.07	(H-2→L)

[a] Owing to the well know overestimate of the CAM-B3LYP functional, the computed excitation energies were red shifted by 0,25 eV to facilitate the comparison with experiment.

[b] Two photon absorption cross-section for linearly polarized light (both photon with parallel polarization).

[c] One photon oscillator strength.